
Imagery Tracking of Sun Activity Using 2D Circular Kernel Time Series Transformation, Entropy Measures and Machine Learning Approaches

Irewola Aaron Oludehinwa^{1,2,*}, Andrei Velichko³, Maksim Belyaev³ and Olasunkanmi I. Olusola²

¹ Department of Physics, Caleb University, Lagos, Nigeria; Irewola.oludehinwa@calebuniversity.edu.ng

² Department of Physics, University of Lagos, Lagos, Nigeria; iolusola@unilag.edu.ng

³ Institute of Physics and Technology, Petrozavodsk State University, 185910 Petrozavodsk, Russia; velichko@petsu.ru; biomax89@yandex.ru

* Correspondence: Irewola.oludehinwa@calebuniversity.edu.ng; Tel.: +2348068030109

Abstract: The sun is highly complex in nature and its observatory imagery features is one of the most important sources of information about the sun activity, space and Earth's weather conditions. The NASA, solar Dynamics Observatory captures approximately 70,000 images of the sun activity in a day and the continuous visual inspection of this solar observatory images is challenging. In this study, we developed a technique of tracking the sun's activity using 2D circular kernel time series transformation, statistical and entropy measures, with machine learning approaches. The technique involves transforming the solar observatory image section into 1-Dimensional time series (1-DTS) while the statistical and entropy measures (Approach 1) and direct classification (Approach 2) is used to capture the extraction features from the 1-DTS for machine learning classification into "solar storm" and "no storm". We found that the potential accuracy of the model in tracking the activity of the sun is approximately 0.981 for Approach 1 and 0.999 for Approach 2. The stability of the developed approach to rotational transformation of the solar observatory image is evident. When training on the original dataset for Approach 1, the match index (T_{90°) of the distribution of solar storm areas reaches $T_{90^\circ} \sim 0.993$, and $T_{90^\circ} \sim 0.951$ for Approach 2. In addition, when using the extended training base, the match indices increased to $T_{90^\circ} \sim 0.994$ and $T_{90^\circ} \sim 1$, respectively. This model consistently classifies areas with swirling magnetic lines associated with solar storms and is robust to image rotation, glare, and optical artifacts.

Keywords: sun; solar storm; solar observatory images; Earth's climate; 2D circular kernel; time series; machine learning; entropy measures; statistical tools;

1. Introduction

The sun has a major impact on Earth: It provides the light and energy that are vital to life on our planet and dramatically shapes Earth's climate. However, the sun's activity is evolving and its dynamics can be in the state of quiet or disturbed. Its disturbances is associated with an intense localized eruption of plasma in form of solar flares [1]. The emanated solar flares are accompanied with coronal mass ejections, solar particle events, and other solar phenomenon that are potentially harmful to spacecraft technology and astronauts in space. To understand the dynamical evolution of the sun's activity and its associated space weather conditions. The imagery from the solar observatory is one of the most important sources of information about the activity of the sun. As a result, the National Aeronautics Space Agency (NASA), Solar Dynamics Observatory (SDO) captures

approximately 70,000 images of the sun activity in a day [2]. Notably, the continuous visual inspection of these solar observatory images regarding the sun activity is challenging. There is need to develop an approach that can automatically detect/track the sun's activity for a more defined and robust search of the space weather. Different methods of classifying, detecting and capturing the activity of the sun have been proposed by several authors using Spectrogram, Image processing, Deep learning, Neural Network, and Machine Learning [2–9]. For instance, in the work of Yang et al. [10] the authors used simulated Annealing Genetic (SAG) method to detect the umbra and penumbra of sunspots simultaneously. Full-disk continuum intensity images obtained from SDO/HMI from May, 2010- December 2016 was used. Their detection results showed that the dual thresholds derived from SAG method have outstanding performance in segmenting the umbra and penumbra from the photosphere with a satisfactory robustness efficiently. Armstrong and Fletcher, [11] applied a deep convolutional neural network to extract features and process images from Hinode/Solar Optical Telescope (SOT). Solar features comprising of filaments, prominence, flare ribbons, sunspots and quiet sun was considered. They reported that the network achieves near perfect performance on classifying unseen images from SOT ($\approx 99.9\%$) in 4.66 seconds and also affirm that the network is robust to changes in resolution by degrading images from SOT resolution (≈ 0.33 at $\lambda = 6563\text{\AA}$) to SDO/AIA resolution (≈ 1.2) without a change in performance of the network. Zhu and Lin, [12] employed a deep learning technique to recognize solar filaments in $H\alpha$ full-disk solar images. They found that the method cannot only identify filaments accurately but also minimize the effects of noise points of the solar images. To overcome the challenge, the authors setup a raw filament dataset consisting of tens of thousands of images required from deep learning. Then, an automated method for filament identification was developed using the U-Net deep convolutional network. They concluded that the cross-validation indicates that the method can effectively identify filament in full-disk $H\alpha$ images. Love et al. [13] used a convolutional neural network (CNN) to analyze the solar observations obtained from the Atmospheric Imaging Assembly (AIA). They identify each image by classifying the shape and position of the flare ribbons into two-ribbon flare, compact/circular ribbon flare, limb flare and where flaring regions are not present. The authors conclude that the network created can classify flare ribbon observation into any of the four classes with 94% accuracy. Sarsembayeva et al. [14] applied an image processing technique to automatically detect active regions of the sun. The image processing technique was based on image enhancement, segmentation, pattern recognition and mathematical morphology. They reported that the identification and classification of sunspots are useful technique for tracking and predicting the solar activity. Abed et al. [15] used a deep learning model based on the integration of convolutional neural network (CNN) and SoftMax classifier to extract special features from the sunspot group images detected from SDO/HMI images. The input data for the model are SDO/HMI full-disk intensity gram images and SDO/HMI full-disk magnetogram images. System outputs are the flare or non-flare of daily flare occurrence. The authors reported that the proposed system achieves a relatively high scores for True Skill Statistics (TSS) and Heidke Skill Score (HSS).

Despite the reports from several authors that had reported different approaches of tracking the activity of the sun from the images of the solar observatory. The concept of transforming the images of solar observatory into 1-Dimensional Time Series (1-DTS) have not been considered in the literatures to the best of our knowledge. The concept has the computational advantage of capturing accurate information regarding the sun activity in the solar observatory image. This observation forms the bedrock of this present study to track the sun activity by capturing the solar storm areas in the sun image, where strong magnetic fields are observed, accompanied by a specific magnetic twisting of the plasma. Therefore, in this study, we developed two approaches of tracking the sun activity from the image of solar observatory using 2D circular kernel time series transformation then extract the information through statistical tools and entropy measures with Machine

Learning (ML) approaches. The block diagram illustrating the two approaches for classifying the areas with strong activity (solar storm) is shown in Figure 1.

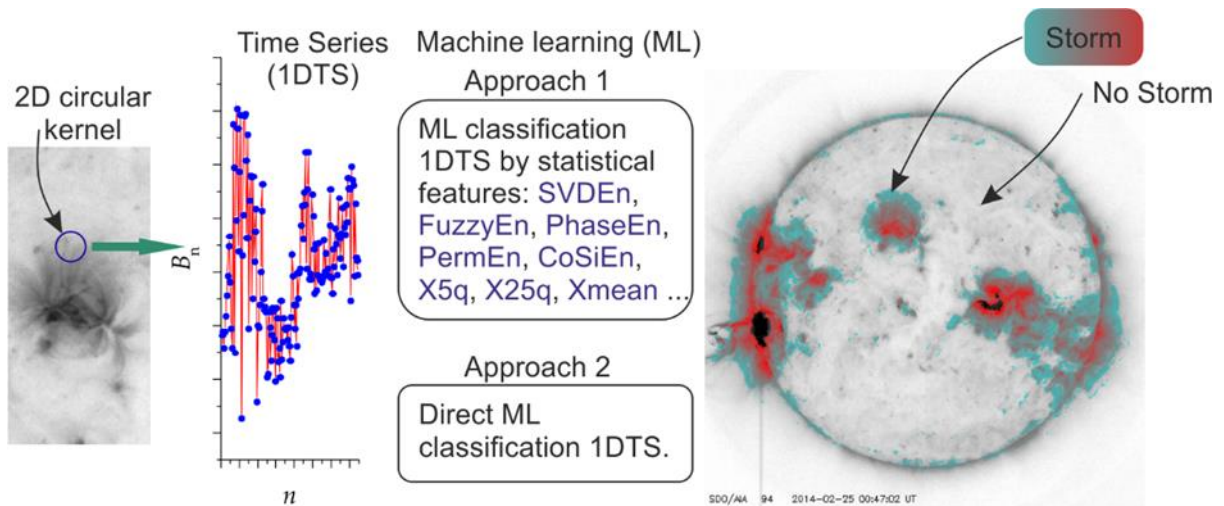


Figure 1. Block diagram of two approaches of sun activity classification using 2D circular kernel time series transformation.

First, a 2D circular kernel with radius $R = 7$ pixels is build which transform the surface area into a 1-Dimensional Time Series. The 1-DTS ($N = 149$) is subjected to statistical and Entropy measures for Machine Learning (ML) classification into two classes 1 and 0 for strong and weak activity of the sun respectively. We called this approach classification by statistical/Entropy measures (Approach 1). The second approach of tracking the sun activity involves using the 1-DTS as an input vector for Machine Learning Classification. Each element of the time series is a kind of micro-feature and we called this approach Direct classification (Approach 2). Therefore, in this study, we present a detailed analysis of the two approaches in capturing the activity of the sun obtained from the images of Solar Dynamics Observatory.

The major contribution of this study are:

- Transformation of the solar observatory images into one-dimensional time series using 2D circular kernel is developed
- Automatic tracking of the sun's activity from the solar observatory image through statistical and entropy measure and machine learning approach is achieved.
- 5th percentile (X_{5P}) and Singular Value Decomposition (SVDEn) depict the best classification accuracy.
- Low entropy is noticed in the solar storm areas while high entropy is associated with no storm areas of the solar observatory image.

The rest of the paper is organized as follows. In section 2, image dataset acquisition and Description of the image data, the method of 2D circular kernel time series transformation, Entropy measures and Machine learning approaches that is employed in this study are explained in details. We present the results in section 3 and discussion in section 4 while the conclusion is drawn in section 5.

2. Materials and Methods

2.1 Description of Image Dataset from Solar Dynamics Observatory

In the study, we consider 5 top solar flares occurrence listed in spaceweatherLive, <https://www.spaceweatherlive.com/en/solar-activity/top-50-solar-flares.html>. Also, we select the 5 days when there is no occurrence solar flares (quiet sun period) shown in Table 1.

Table 1. The list of selected solar storm and quiet Events used in this study

S/N	Solar Storm Events	Time of Occurrence (UT)	S/N	Quiet Event	Time of Occurrence (UT)
1	2013/05/13	16:17	6	2019/12/15	01:15
2	2013/05/13	01:02	7	2019/12/16	12:29
3	2014/02/25	00:47	8	2019/12/17	01:59
4	2017/09/06	11:59	9	2020/03/03	00:14
5	2017/09/10	16:00	10	2020/06/06	01:04

The solar observatory images of the selected days were obtained from the archive of NASA, Solar Dynamic Observatory (SDO), <https://sdo.gsfc.nasa.gov/data/ai-ahmi/browse/queued.php>. The images were Atmospheric Imaging Assembly (AIA) 094 format in green colors. Furthermore, we considered the time when the emergence of solar flares occurs and its observatory images was collected. Ten images corresponding to different solar activity of 512×512 size pixels was used in this study (See Supplementary material). We display in Figure 2a,b the samples of images of the sun depicting the weak and strong sun activity. While Figure 2c is the sample of solar image for strong solar activity that is converted to grayscale format. Using the RGB color palette conversion, the JPG color images of the sun obtained from the SDO were converted to grayscale format with gradation of brightness according the formula below:

$$B_{x,y} = 0.3RGB R_{xy} + 0.59RGB G_{xy} + 0.11RGB B_{xy} \quad (1)$$

Where x, y are pixel coordinates.

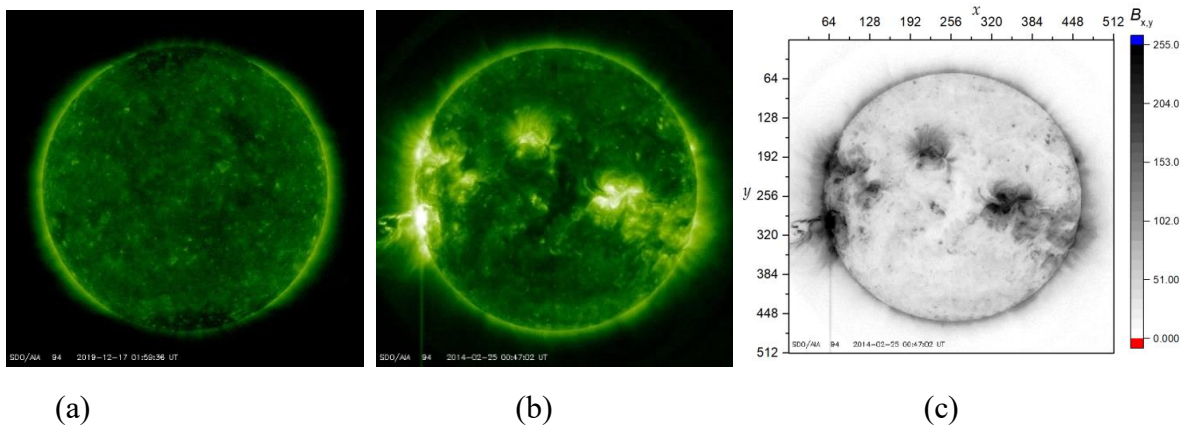


Figure 2. Sample of images of the sun with (a) weak activity (b) strong activity and (c) the image of strong solar activity converted to grayscale format.

2.2 Method for 2D Circular Kernel Time Series Transformation of Solar Observatory Images

The concept of using circular kernel to calculate the 2D entropy was developed by Velichko et al. [16,17]. Its essence lies in the transformation of a 2D image area using circular kernel of a radius R into a 1-dimensional time series. Areas that are outside the image boundaries are not defined, so the pixel values in these areas are filled by the symmetrical mirroring of the pixel in the image. While the set of pixels inside the local kernel is converted into one-dimensional time series data. The number of pixel (N) in a circular kernel has a quadratic dependence on the radius [16]. To obtain the one-dimensional time series for the solar observatory images, we apply a circular kernel of radius ($R = 7$) and the number of pixels is $N = 149$. Then, the algorithm traced the pixel along the connecting line starting from the center of the kernel ($N = 1$) and ending with element ($N = 149$) leading to the formation of elements of the time series, see Figure 3. The first element of the series is always equal to the brightness value of the central pixel, relative to which the circular core is located. Transformation through the circular kernel was applied to all the pixels of each solar observatory images used in this study. We obtained from the first image $512 \times 512 = 262144$ time series. For each time series, the statistical characteristics were estimated and the 2D distribution of entropy measures and other characteristics were built. The entropy distribution is denoted by $SVDEN_{2D}$, $FuzzyEN_{2D}$, $PhaseEN_{2D}$, $PermEN_{2D}$, and $CosiEN_{2D}$.

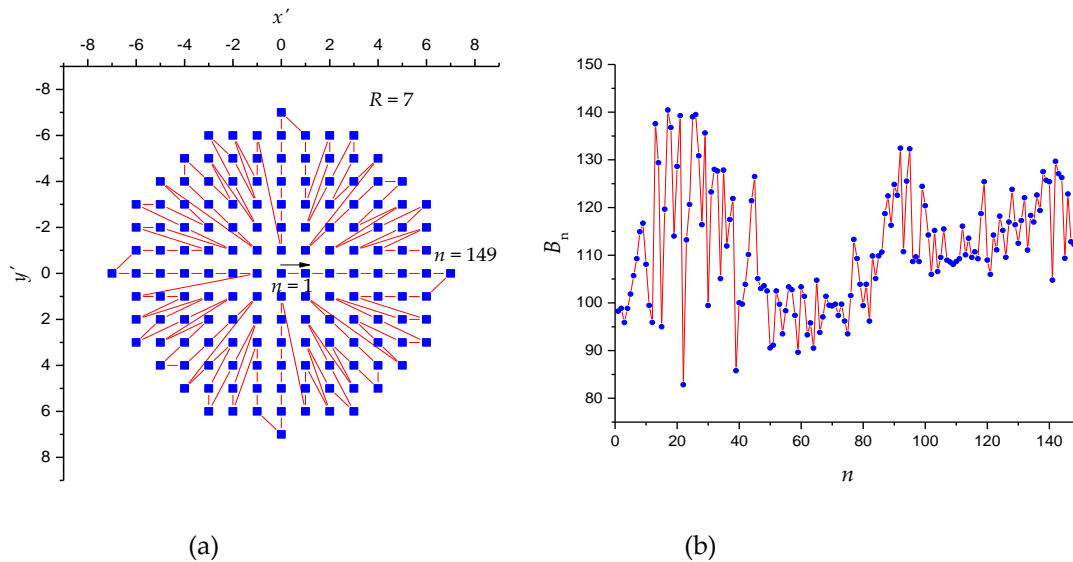


Figure 3. Scheme for converting a two-dimensional pixel distribution into a one-dimensional data series ($R = 7$).

2.3 The Method for Creating Training Dataset

2.3.1. The Original Dataset

The original dataset used for training and testing the models contained 25735 time series data points. Of which 3451 1-DTS belong to the regions with strong magnetic field corresponding to a solar storm (Class 1-storm) and 22284 1-DTS belong to the region with no magnetic anomalies (class 0-No storm). The dataset was obtained from the 10 solar observatory images used in this study. We illustrate in Figure 4, the images of the solar observatory unveiling the position of the training dataset pixels. The pixels marked in red colour correspond to the areas with strong magnetic field while the blue colour correspond to the region with no magnetic anomalies. The red pixels were set based on the presence of magnetic field lines while the illuminated areas of the image with no pattern of magnetic field lines were marked in blue colour. Table 2 show the number of points in the categorize classes (i.e., class 1-storm, class 0-No storm) for all the solar observatory images. The total number of pixels for all the 10 images contain $10 \times 512 \times 512 = 2621440$ pixels, of which 25735 pixels are marked as either class 1 or class 0, which correspond to

about 1%. Thus, the marked points make up a small fraction of all image points. The classification result of the remaining 99% of the image area will be presented in the result section.

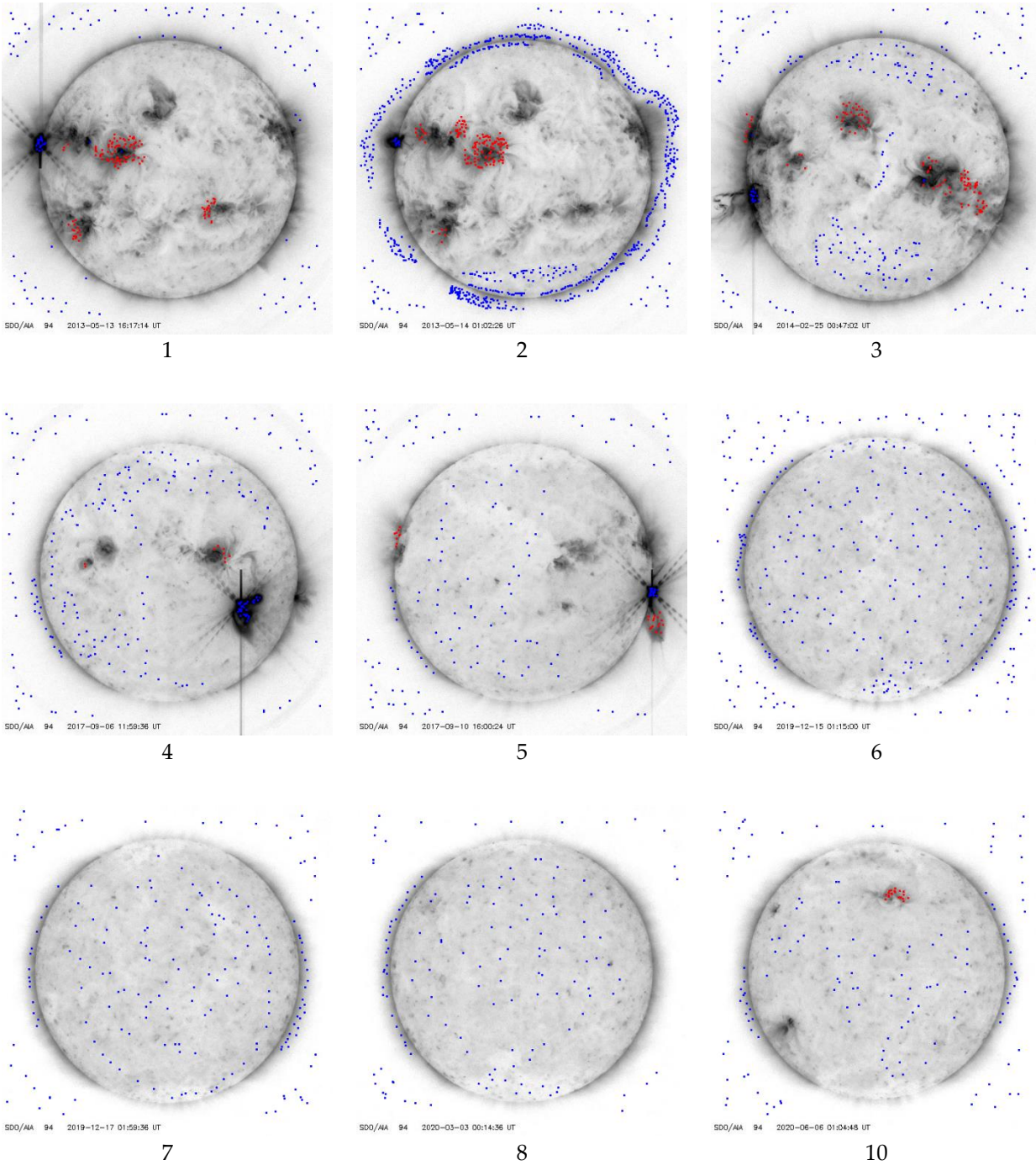


Figure 4. The position of the training dataset pixels on the images of the sun obtained from solar observatory. Pixels are marked in red, corresponding to areas with a strong magnetic field (Class 1 - Storm) and in blue without magnetic anomalies (Class 0 - No Storm). Image numbers are used to indicated image filename shown in Table 2.

Table 2. Number of labeled pixels in the image of the solar observatory used in this study

Number of image №	Image file name	Number of labeled pixels	
		Class 1 - Storm	Class 0 - No Storm
1	Solarflare20130513_161714_512_0094.jpg	967	989
2	Solarflare20130514_010226_512_0094.jpg	1112	7461
3	Solarflare20140225_004702_512_0094.jpg	895	1909
4	Solarflare20170906_115936_512_0094.jpg	81	1946
5	Solarflare20170910_160024_512_0094.jpg	222	1294
6	Solarflare20191215_011500_512_0094.jpg	0	2805
7	Solarflare20191216_122948_512_0094.jpg	0	1786
8	Solarflare20191217_015936_512_0094.jpg	0	1623
9	Solarflare20200303_001436_512_0094.jpg	0	1274
10	Solarflare20200606_010448_512_0094.jpg	174	1197

2.3.2 The Extended Dataset

The need for an extended dataset arises, if it is necessary to improve the quality of the training and to make the classification more invariant to image rotation. The extended dataset was generated from the original dataset by adding 1-DTS of appropriate 90° , 180° , and 270° rotational transformations. The 1-DTS rotational transformation is generated by shifting the element of the time series in a circle, starting from the second element. For instance, to turn 90° clockwise, we sweep all the elements of the 1-DTS, 37 steps to the right, see Figure 5. This becomes possible due to the shape of the 2D circular kernel described in Figure 3, which has rotational symmetry. Therefore, the extended dataset consists of $25735 \times 4 = 102940$ time series. The pixel $3451 \times 4 = 13804$ 1-DTS belong to the region with a strong magnetic field corresponding to a solar storm (class 1-storm) and $22284 \times 4 = 89136$ 1-DTS corresponds to the region with no magnetic anomalies (class 0-No storm).

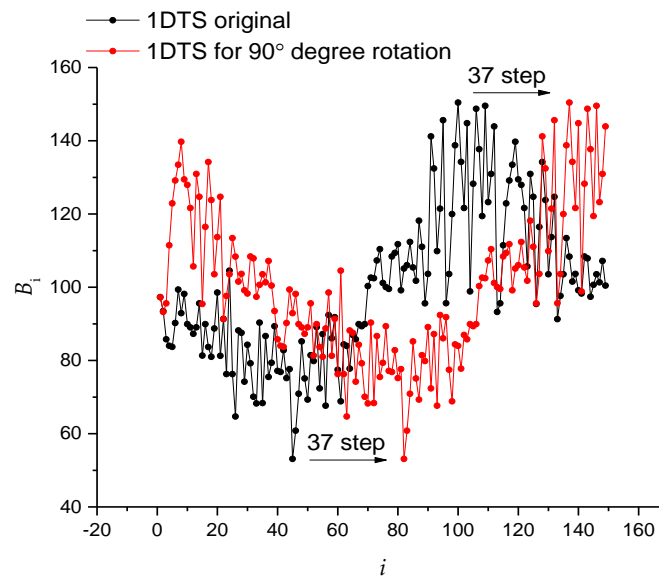


Figure 5. 1-DTS element displacement principle for emulating rotational image transformation by 90° clockwise

2.4 The One-Dimensional Time Series Classification Methods

We employ two approaches of classification to the time series obtained from the images of the solar observatory. The first approach is traditional which applies various statistical and entropy measures to capture the information in the image of the sun and we called this approach classification by statistical tools and entropy measures. The second approach applies all the elements of the time series as micro-features and called this approach Direct classification. In this approach, we consider approximating a hypothetical function to determine a solar storm region in the images of the sun using machine learning methods. The two approaches implement preprocessing, cross-validation and classification. Only at the stage of capturing the information of the solar images differs.

2.4.1. Classification by Statistical tools and Entropy Measures (Approach 1)

Statistical tools comprising of Mean Value (X_{mean}), Median Value (X_{med}), Standard deviation (X_{std}), Variance (X_{var}), 5th Percentile (X_{5P}), 25th Percentile (X_{25P}), 75th Percentile (X_{75P}), 95th Percentile (X_{95P}), Root mean square (X_{rms}), Skewness (X_{sk}), and Kurtosis (X_{kt}), were employ to extract the information in the solar observatory images through classification of the time series. They are popular tools used to identify the pattern and trend of a dataset. We refer interested readers to the work of Ali and Bhasker, [18] where the mathematical formulation of the statistical tools used in this study is explained in details. Entropy measures are essential statistical tool used to measure the irregularity or randomness of a time series data. The measure of entropy serves as an index to measure the complexity of a dynamical system [19–21]. Its concept is developed from information theory and have been proven to be a potentially useful tools in change detection and image quality assessment. Application of image processing through entropy measures have been proposed by Velichko et al. [16,17] in remote sensory and is considered as an irregularity measure for images. Entropy measures have different mathematical and computational steps in determining entropy values.

Singular Value Decomposition Entropy (SVDEn): Is an entropy measures that applies orthogonal matrix decomposition method and has been widely used in signal detection by different authors [22,23]. It involves reconstruction of phase space in which one-dimensional time series is converted into m -dimensional vectors through embedding theorem and perform a singular value decomposition (SVD) of trajectory matrix in order to further decomposed the vectors into the sum of rank-one elementary matrix. The mathematical steps is described as follows: given a time series,

$$Y = [Y_1, Y_2, \dots, Y_i, \dots, Y_N] \quad (2)$$

Introducing an embedding theorem to the time series, a phase space reconstruction is form as

$$U_i = [Y_i, Y_{i+n}, \dots, Y_i, \dots, Y_N] \quad (3)$$

Where n is the time delay, m is the embedding dimension. Then, the embedded vector (U) is subjected to a singular Value Decomposition (SVD).

$$U = C \Sigma V^T \quad (4)$$

Where $C(N - (m - 1)n \times N - (m - 1)n)$ and $V(m \times m)$ are orthogonal, the m elements $\sigma_1 \geq \sigma_2 \geq \dots, \geq \sigma_m$ of the diagonal matrix Σ are the singular values of U . Therefore, the first singular values can be quantified by

$$SVDEn = -\sum_{i=1}^m \bar{\sigma}_i \log_2 \bar{\sigma}_i \quad (5)$$

Where $\bar{\sigma}_i = \frac{\sigma_i}{\sum_{j=1}^m \sigma_j}$ is the normalized singular values. In this study, the 1-DTS obtained from the solar observatory image was subjected to SVDEn using the computation parameters of embedding dimension $m = 3$ and delay $n = 1$.

Permutation Entropy (PermEn): as a nonlinear dynamics tool was introduced by Bandt and Pompe, [24] which estimate the complexity parameters for the time series rather than the values themselves. The method of permutation entropy has the advantage of simplicity and robustness in the presence of observational and dynamical noise compared to approximate entropy and sample entropy. It is mathematically expressed as:

$$PermEn = -\sum P_i \log_2 P_i \quad (6)$$

Where P_i is the frequency of occurrence of the i -th permutation in the embedded matrix U , which is expressed in the same procedure as in equation 5. We compute the permutation entropy using the embedded dimension $m = 5$ and $n = 1$ for the analysis of our study.

Cosine Similarity Entropy (CosiEn): Is another form of entropy measure that employ angular distance to estimate the similarity between embedding vectors instead of the Chebyshev distance while the conditional entropy is replaced with the Shannon entropy [25–27]. This concept was introduced by Chanwimalueang and Mandic, [25] to analyze dynamical systems. The cosine similarity entropy is expressed as follows: For a given time series data expressed in form of equation 2. Introducing embedding dimension (m), tolerance (r) and delay (n), a phase space reconstruction is form similar to equation 3. Then, the angular distance for all pairwise embedding vectors is computed as:

$$AngDis_{i,j}^{(m)} = \frac{1}{\pi} \cos^{-1} \left(\frac{Y_i^{(m)} \cdot Y_j^{(m)}}{|Y_i^{(m)}| |Y_j^{(m)}|} \right) \quad i \neq j \quad (7)$$

The number of similar patterns, $P_i^{(m)}(r)$ is obtained when a criterion $AngDis_{i,j}^{(m)} \leq r$ is fulfilled. The local and global probability of similar patterns, $B_i^{(m)}(r)$ and $B^{(m)}(r)$ are calculated as:

$$B_i^{(m)}(r) = \frac{1}{(N-n-1)} P_i^{(m)}(r) \quad (8)$$

$$B^{(m)}(r) = \frac{1}{N-n} \sum_{i=1}^{N-m} B_i^{(m)}(r) \quad (9)$$

Therefore, cosine similarity entropy is now estimated as:

$$CosiEn = -\left[B_{(r)}^{(m)} \log_2 B_{(r)}^{(m)} + (1 - B_{(r)}^{(m)}) \log_2 (1 - B_{(r)}^{(m)}) \right] \quad (10)$$

The embedding dimension $m = 2$ and the tolerance $r = 0.1$ was used in the computation of cosine similarity entropy.

Phase Entropy (PhaseEn): Is a new method of entropy measure that quantifies the distribution of the time series data in phase space representation. The algorithm considers the slope of each scatter point from the origin of phase space representation and divides the entire phase portrait into sections have an angle of $2\pi/k$ radian each [28]. The cumulative slope of each sector is then obtained by adding the slope of each scatter point within that sector. Finally, the probability distribution of the slopes in each sector is calculated through Shannon entropy to give the phase entropy.

$$PhaseEn = -\frac{1}{\log k} \sum_{i=1}^k P(i) \log P(i) \quad (11)$$

Fuzzy Entropy (FuzzyEn): measures entropy based on fuzzily defined exponential functions for comparison of vectors similarity instead of Heaviside function used by Approximate entropy and Sample entropy to calculate the irregularities in a time series data

[29]. Fuzzy entropy can be calculated as follows: for a given time series $x(n) = [x(1), x(2), \dots, x(N)]$ with given embedding dimension (m), an $m - vectors$ is form as:

$$X_m(i) = [x(i), x(i + 1), \dots, x(i + m - 1)] - x_0(i) \quad (12)$$

These vectors represent m consecutive x values, starting with ith point, with the baseline $x_0(i) = \frac{1}{m} \sum_{j=0}^{m-1} x(i + j)$ removed. Then, define the distance between vectors $X_m(i)$ and $X_m(j)$, $d_{ij,m}$ as the maximum absolute difference between their scalar components. Given n and r , the degree of similarity $D_{ij,m}$ of the vectors $X_m(i)$ and $X_m(j)$ is calculated using fuzzy function.

$$D_{ij,m} = \mu(d_{ij,m}r) = \exp\left(-\frac{(d_{ij,m})^n}{r}\right) \quad (13)$$

Define the function ϕ_m as:

$$\phi_m(n, r) = \frac{1}{N-m} \sum_{i=1}^{N-m} \left(\frac{1}{N-m-1} \sum_{j=1, j \neq i}^{N-m} D_{ij,m} \right) \quad (14)$$

Also, the dimension to $m + 1$, form vectors $X_{m+1}(i)$ and obtain the function ϕ_{m+1} by repeating the same procedure from equation (13-14). Therefore, FuzzyEn can be estimated as:

$$FuzzyEn(m, n, r, N) = \ln \phi_m(n, r) - \ln \phi_{m+1}(n, r) \quad (15)$$

In the computation of fuzzy entropy, the embedding dimension $m = 1$ and tolerance $r=0.05 \times \text{std}$, where std is a standard deviation of $x(n)$, was used in the analysis. This statistical tools and entropy measures were used individually and all together to examine the contribution of this tools to the classification of the 1-DTS obtained from the solar observatory images.

2.4.2 Direct classification by Machine Learning (Approach 2)

In this approach, the original or extended datasets were used for training set explained in section 2.3 and the time series vector containing $N = 149$ element was feed directly to the input of the machine learning (ML) classifier

2.4.3 Data Preprocessing

Regardless of the training data set, the values of the features used were standardized. It was carried out by subtracting the mean value of the feature, and dividing by its standard deviation. Therefore, after standardization, the elements of each feature have zero mean and unit variance.

2.4.4. Cross-Validation

Classification accuracy was assessed using the Support Vector Classifier (SVC) and K-Nearest Neighbors (KNN) methods by using the scikit-learn module. The classification accuracy assessment consists of two successive stages. At the first stage, the hyperparameters of the models were selected using K-fold cross-validation. To implement this, the training dataset was divided into $K = 10$ blocks. At the same time, the distribution of classes in each K-block approximately correspond to the distribution in the original dataset. Therefore, the blocks form training and validation sets. Notably, each of the K-blocks undergo validation 1 time, and the remaining 9 times were included in the training set. Then, the values of the classifier hyperparameters were selected, which maximized the average value of the target metric (F1) on the validation set. The resulting average value of the target metric may be too optimistic, due to the optimization of hyperparameters on a fixed set of samples. After determining the optimal hyperparameters, the second stage involving cross-validation is then performed using other 5 partitions into $K = 10$ blocks. The value of the target metric $F1_{KF}$, averaged over 5 partitions, obtained on new partitions, was used as an estimate of the accuracy of the classifier.

2.4.5 Image classification

The most accurate models obtained were used to process the solar observatory images. The result of the classification is displayed as a red color superimposed on the main color of the pixel by the XOR operation.

$$colour = Base(colour) XOR Red(colour) \quad (16)$$

As a result, area of the pixel with a solar storm were painted in shades of blue and red colors. The red tint is mainly obvious in the center of the solar storm, see Figure 6a, because there is greatest brightness of the magnetic lines in this region, while the blue tint corresponds to the magnetic lines of less intensity. For comparison, we display in Figure (6b) the color marking using without XOR operation, which, in our opinion, is less informative when analyzing images of the solar observation.

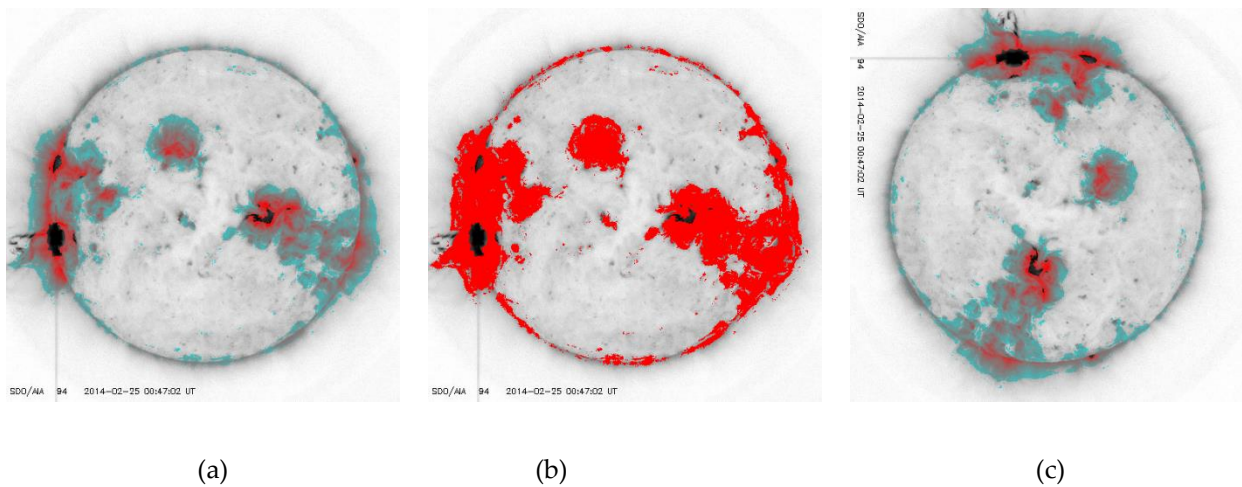


Figure 6. A sample of the result of image classification for no.3 in color with XOR (a) and without XOR (b), after rotation with XOR (b).

2.5.6 Methods for testing the stability of models to rotational transformation

To test the robustness of the models to rotational image transformation, the image of the solar observatory was rotated 90° clockwise (Figure 6c) and reclassified. The match of the result was evaluated by the match index T_{90^0}

$$T_{90^0} = \frac{\text{Number of matching classifications}}{512 \times 512} \quad (17)$$

The T_{90^0} index is the ratio of the number of matching classifications to the total number of pixels.

3. Results

3.1. The Results from Classification of Solar Observatory Images Using Statistical tools and Entropy Measure (Approach 1)

We present in Table 3, the values of the classification accuracy for original database whose features extraction were obtained from individual statistical tools, individual entropy measures. Also, the classification of all the entire statistical tools altogether and the entire entropy measure altogether. The results from the table revealed that the strongest feature extraction obtained from the statistical and entropy measure is the 5th percentile (X_{5p}) with classification accuracy $F1_{KF}$ of 0.918. In addition, the result obtained from the mean value (X_{mean}) also depicts strong value of feature extraction. Among the entropy

measures, the feature extraction obtained from SVDEn had a higher value of classification accuracy $F1_{KF} \sim 0.681$. Comparatively, the feature extraction obtained from the statistical tools collectively gives a higher value of classification accuracy $F1_{KF} \sim 0.955$ compared to the collective entropy measures classification accuracy $F1_{KF} \sim 0.891$. This observation signifies that the statistical tools possess the potential to track more accurate features extraction from the images of the solar observatory.

Table 3. Classification results according to the original database using the KNN classifier.

Feature	$F1_{KF}$	Feature	$F1_{KF}$
	Original dataset		Original dataset
SVDEn	0.681	X_{med}	0.91
FuzzyEn	0.272	X_{75p}	0.9
PhaseEn	0.268	X_{std}	0.388
PermEn	0.184	X_{var}	0.388
CoSiEn	0.122	X_{sk}	0.328
X_{5p}	0.918	X_{kt}	0.194
X_{25p}	0.914	All entropy features	0.891
X_{mean}	0.913	All statistical features	0.955
X_{rms}	0.913	All features	0.977
X_{95p}	0.91		

Regarding the implementation of Support Vector Classifier (SVC) for the entire set of statistical and entropy measures. We notice that the value of the classification accuracy $F1_{KF} \sim 0.891$ for SVC is higher in comparison to K-Nearest Neighbor (KNN). This suggests that the SVC gives the most accurate model in obtaining features extraction through the statistical and entropy measures after training and we implement the SVC to the images of the solar observatory. The results are shown in Figure 7, and the visual inspection of the analysis shows that the model accurately tracks the areas with occurrence of solar storms, where magnetic lines are clearly visible in the images of the solar observatory (See Figure 7, image no 1, 2, 3, 4, 5 and 7). Furthermore, the model also identifies the solar storm areas where none of the points from the original database were found, See (Figure 7, images no 1, 2 and 9). This further strengthened the effectiveness and robustness of the model in tracking the activity of the sun from the solar observatory images. On the solar observatory images, where there are quiet activities of the sun (i.e., no occurrence of solar storm at all), the model did not highlight any feature in the images of the sun obtained from the solar observatory shown in (Figure 7, image no. 6, 7, and 8). The classification time for all the 512×512 pixels obtained from the solar observatory is about 16 minutes using SVC classifier. Notably, the entropy measures spent most of the computational time on each 1-DTS obtained from the solar observatory images.

The stability checking of the model to rotational transformation revealed a match index $T_{90^\circ} \sim 0.9939$ when image no 3 of the solar observatory is rotated 90% clockwise as shown in Figure 6. The value of the match index $T_{90^\circ} \sim 0.9939$ signifies that the model is robust to stability of the feature extraction obtained from the statistical and entropy measures to rotational transformation. Remarkably, the values of the statistical tools do not depend on rotation, because the elements in the time series only change their order within the series. However, entropy measures change their values from the permutation of elements in the time series. The results of the match index (T_{90°) using extended database showed a slight increase $T_{90^\circ} \sim 0.9942$. This further strengthened the efficiency of the model and allows a relatively small training database to implement a complete classification of solar observatory imagery pixels and captures the areas of the solar storm.

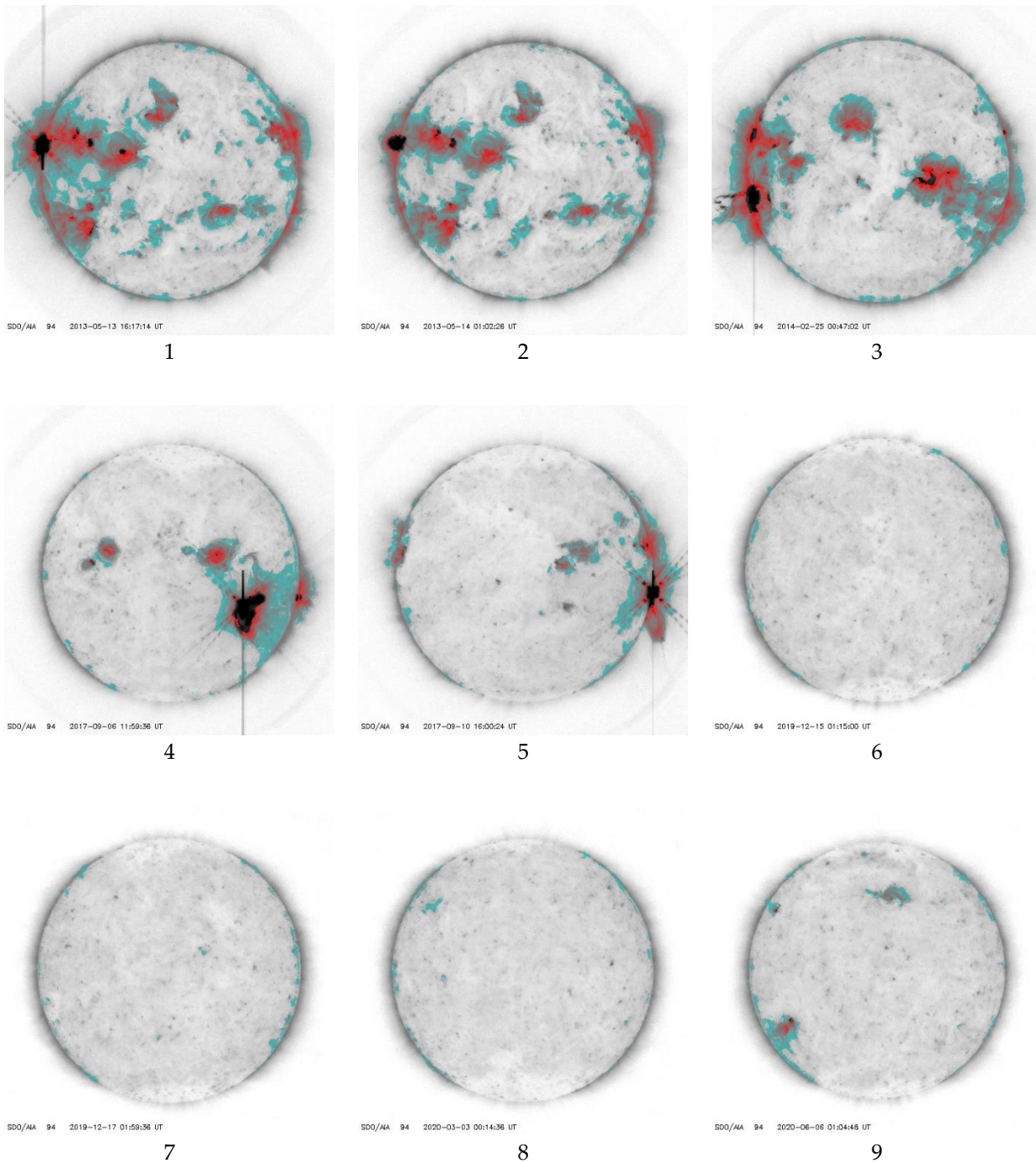


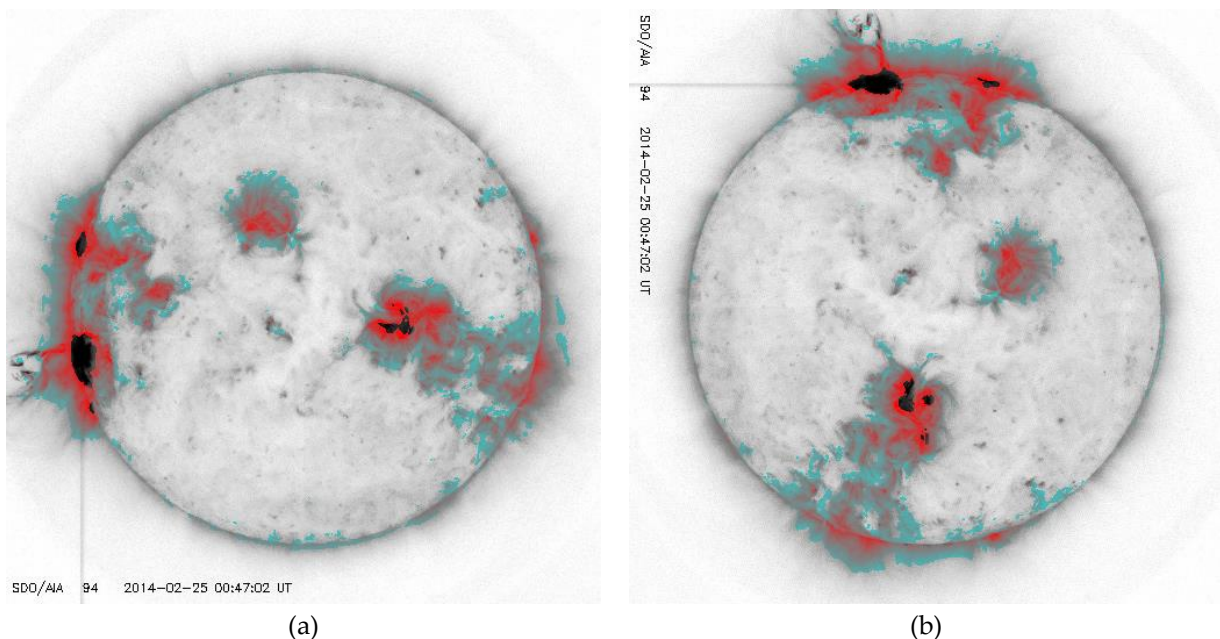
Figure 7. The results of applying the SVC classifier on the solar observatory images after training on the original database (Approach 1). The numbers below indicate the image number of solar observatory.

3.2 The Results from Classification of solar observatory images using Direct time series classification (Approach 2)

The result of the direct classification method for the original database using KNN classifier showed a classification accuracy of $F1_{KF} \sim 0.999$ while the SVC classifier model revealed 0.998 classification accuracy. This high value of classification accuracy for both KNN and SVC classifier unveils the potential of the Direct Classification method in that it

enables one to achieve a better accuracy on the training compared to the method of classification using statistical and entropy measures. We display in Figure 8a, the image of the solar observatory depicting strong solar activity of the sun. This image processed using the KNN model shows that the model captures similar distribution of solar storm areas in the solar observatory images as obtained in the method of classification using statistical and entropy measures (See Figure 7, image no 3). The classification time through the direct classification method for all the pixels 512×512 solar observatory images is 1 minutes using SVC. This implies that the computation time of the direct time series classification method is much lesser than the computation time for classification through statistic and entropy measures.

The stability checking for the direct time series classification method to rotational transformation showed that the match index T_{90° is 0.9516. We display in Figure 8b, the result of the classification, when the image of the solar observatory is rotated 90° clockwise. Our findings revealed that the value of T_{90° is lower than the match index of classification using statistical and entropy measures. This shows that the direct time series classification model on the original base is less resistant to rotational transformation. This is because the time series at the input is shifted during image rotation (see Figure 5), and KNN main criterion is the distance metric between the group of vectors. Furthermore, the stability checking of the direct classification model to rotational transformation after training on the extended database revealed a significant increase in the match index $T_{90^\circ}=1$. Thus, suggesting that adding more samples of rotation to the training database significantly improves the functionality of the direct time series classification model. In Figure 8c,d we display the classification result at before and after rotation. We noticed that after the rotation, the distributions of solar storm areas coincide completely. In addition, the direct time series classification model is resistant to optical artifacts in the form of straight lines and the image flare, see Figure 8a.



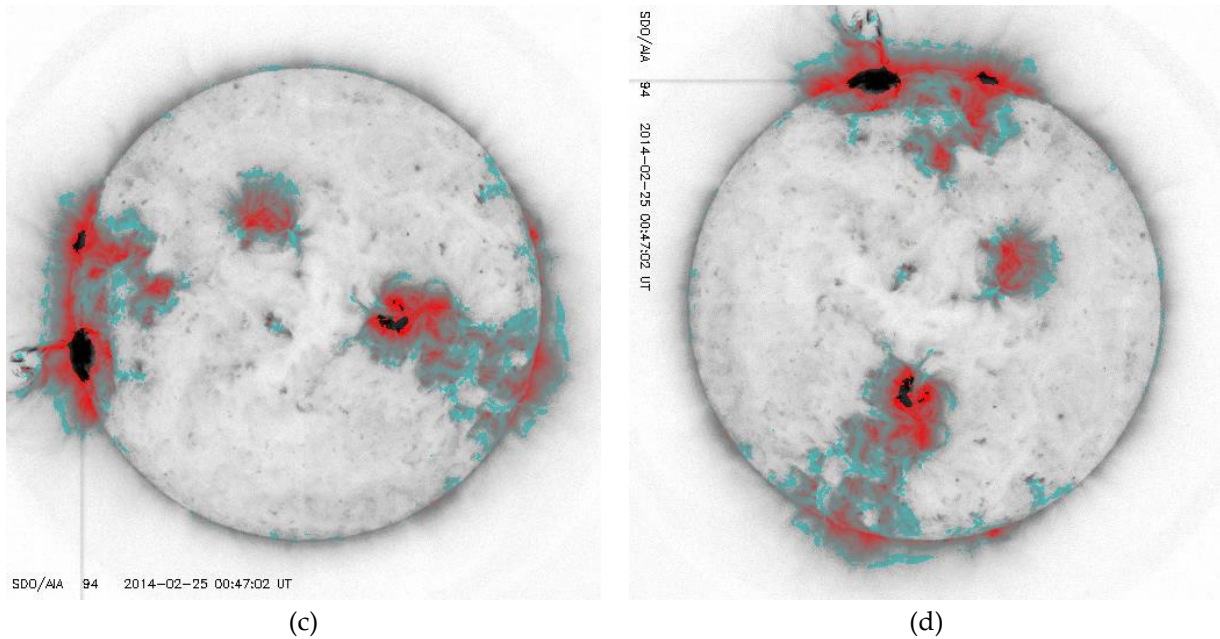


Figure 8. The results of applying the KNN classifier (Approach 2) in image no 3, after training on the original base before (a) and after rotation (b) $T_{90} \sim 0.9516$. (c) is results of applying the KNN classifier in image No3, after training on the extended base before and (d) is the result of KNN classifier in image no 3 after rotation ($T_{90} = 1$).

3.3 Peculiarities of the Time Series Obtained from the imagery areas with Solar Storm

The results of the previous subsection have explained how applicable the two developed approaches track the areas of a solar storm from the image of the sun obtained from the solar dynamics observatory. However, there is need to shed more light on the cause of this dependence. In addition, to explain the underlying dynamics of the time series obtained from the solar observatory images corresponding to the state of solar storm and no solar storm. We display in Figure 9a,b a section from the area of a solar storm and no solar storm in the image of the solar observation, see (Figure 9a, where the section is obtained from image no 3). While the Figure 9b depicts the obtained time series from the image of the sun. The pixels belonging to the training database are marked in red and blue colors. The red pixel is numbered 1 and 2 belonging to the areas of solar storm while the blue pixels numbered 3 and 4 belong to the areas without a solar storm. The time series from these areas is shown in Figure 9b. We observe that the trend of the time series obtained from points 1 and 2 depicts an increase value in amplitude with a characteristic wavy pattern of amplitude changes. The time series obtained from points 3 and 4 is noticed to depict a reduced amplitude with no periodic patterns and exhibits more chaotic dynamics. This suggest that the better the statistical and entropy measures capture the patterns of amplitudes and the inherent time series pattern obtained from the 1-DTS of solar storm areas, the better the classification of the Machine Learning (ML) classifier.

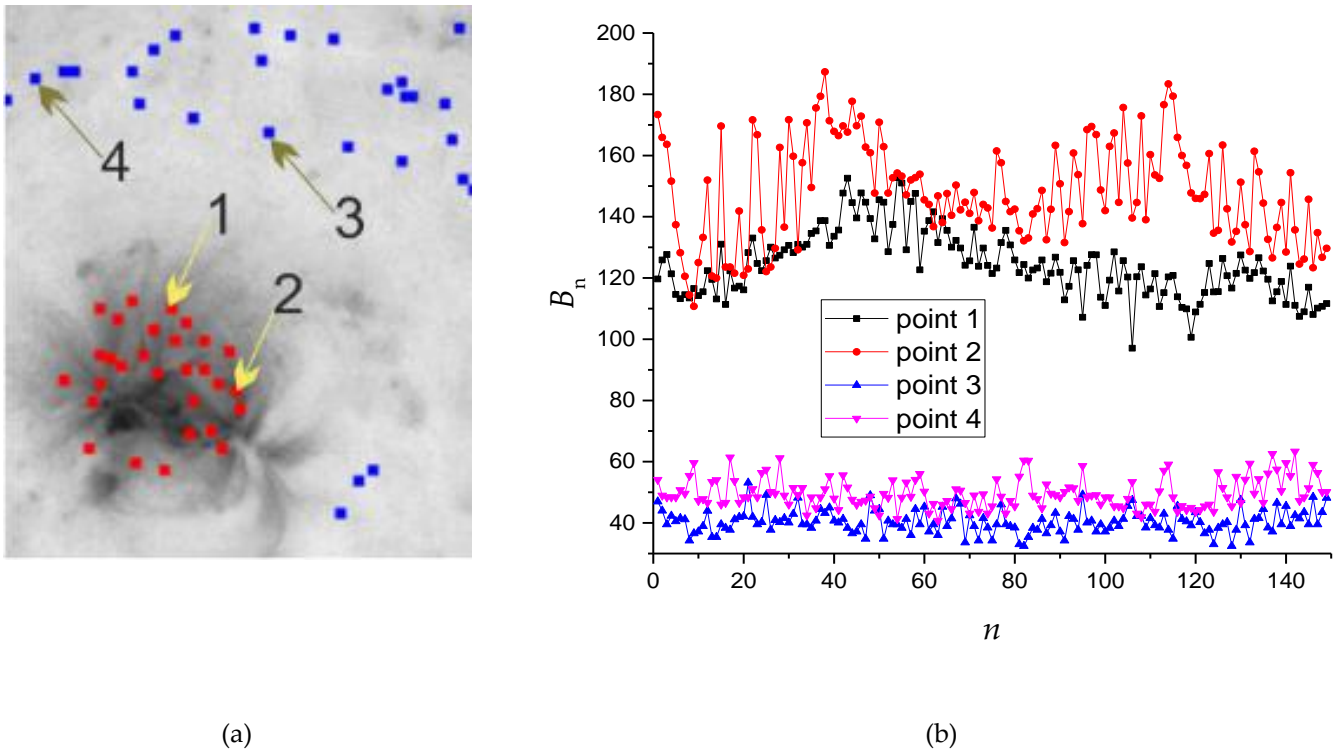
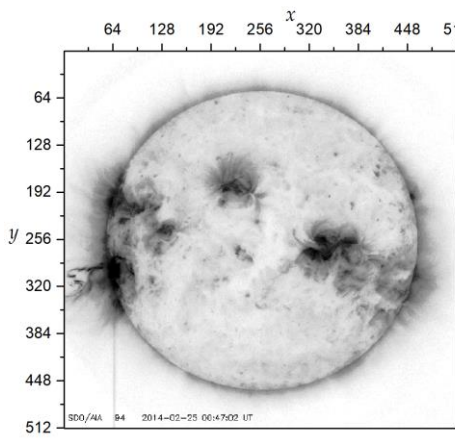
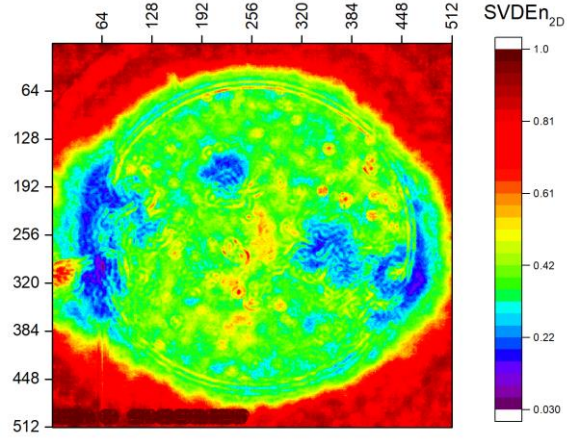


Figure 9. The pixel of the marked areas of solar storm and no solar storm in the image of solar observation (a) and (b) depicting the time series pattern of the marked pixel. The Red pixel indicate the solar storm areas while the blue color mark the no solar storm area

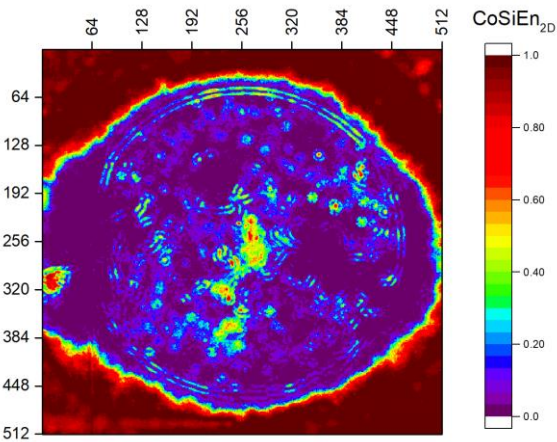
Figure 10 a-h shows the distribution of the feature extraction obtained from the solar observatory image through statistical tools and entropy measures. Figure 10a is the solar observatory image no 3 while Figures 10b-f represent the feature extraction distribution obtained through entropy measures comprising of $SVDEn_{2D}$, $Cosien_{2D}$, $PhaseEn_{2D}$, $FuzzyEn_{2D}$ and $PermEn_{2D}$. Finally, Figure 10g-h depict the feature extraction distribution obtained through statistical tools of 5th percentile (X_{5P}) and standard deviation (X_{std}). We notice that the $SVDEn_{2D}$ (See Figure 10b) depicts low values of entropy in the areas of solar storm. This may be attributed to the periodicity of the time series pattern obtained in the solar storm areas and the increased amplitude. Notably, the entropy obtained from $SVDEn_{2D}$ has the highest classification accuracy $F1_{KF} \sim 0.681$ compared to other entropy measures used in this study, see Table 2. This signifies that the $SVDEn_{2D}$ is the best entropy measure to capture feature extraction embedded in the solar observatory images. The strongest feature extraction that captures the solar storm areas in the image of the solar observatory is observed in the (X_{5P}) distribution shown in Figure 10g. The X_{5P} is the value that the elements of the time series do not exceed with a probability of 5%. An interesting fact is that it possesses the characteristic of practically eliminating the presence of alpha-numeric at the bottom of the images of solar observatory. In addition, the feature extracted correlates very well with the presence of a solar storm. The distribution of X_{5P} is also another statistical tool that is also sensitive of a solar storm, with elevated values in these areas. This is apparently due to a strong change in the amplitude of the time series in the solar storm shown in Figure 9b for points 1 and 2.



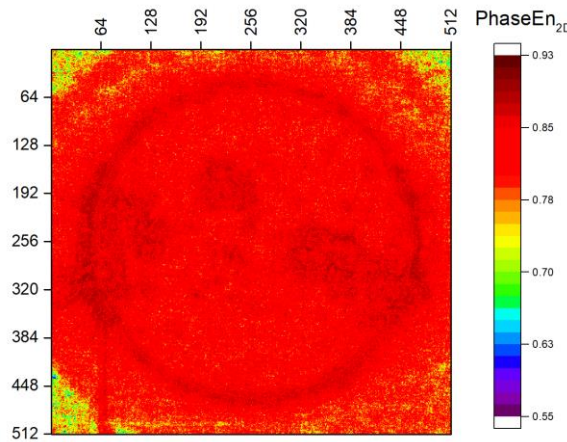
(a)



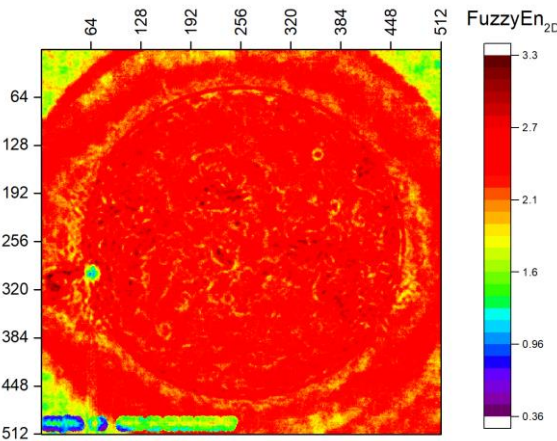
(b)



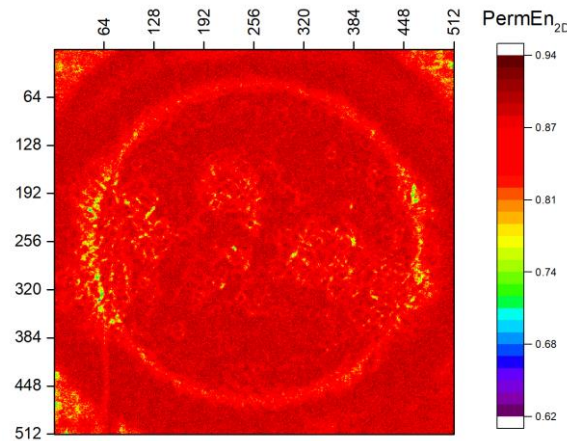
(c)



(d)



(e)



(f)

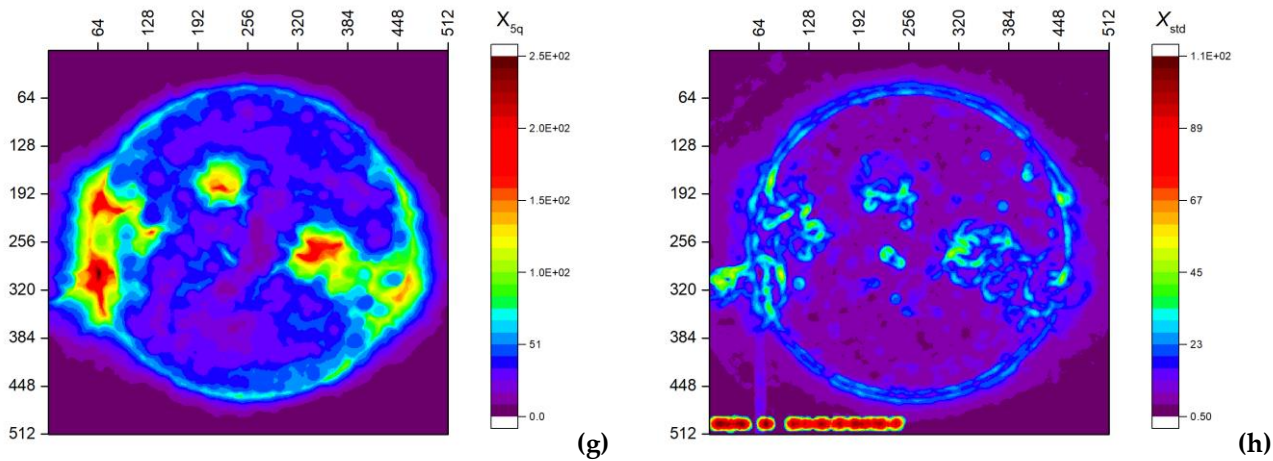


Figure 10. The distribution of the feature extraction obtained from the solar observatory image, no. 3 through statistical tools and entropy measures (a) is the gray color of solar observatory image, no.3, (b) SVDEn_{2D} distribution (c) CosiEn_{2D} distribution (d) PhaseEn_{2D} distribution (e) FuzzyEn_{2D} distribution (f) PermEn_{2D} distribution (g) X_{5P} distribution (h) X_{std} distribution

4. Discussion

The classification accuracy of the solar observatory images through the statistical and entropy measures revealed that the feature extraction captured from the 1-DTS of the solar observatory images using 5th percentile (X_{5P}) and mean value (X_{mean}) depict high value of classification accuracy compared to standard deviation (X_{std}), Variance (X_{var}), 75th percentile (X_{75P}), and 95th percentile (X_{95P}). Its implies that the (X_{5P}) and (X_{mean}) are potentially useful statistical tools to capture the feature extraction from the 1-DTS obtained from the solar observatory images. Furthermore, the result obtained from the entropy measures show that the SVDEn (2-5) depict the highest value of classification accuracy compared to FuzzyEn (12-15), PhaseEn (11), PermEn (7-10), and CosiEn (7-10). This actually unveil the potential of the SVDEn to capture precise information from the 1-DTS obtained from the solar observatory images. However, the feature extraction obtained through the statistical tools give more information about the state of the activity of the sun in the solar observatory image compared to the entropy measures. This is an indication that the statistical tools and entropy measures are strong diagnostics tool in tracking accurate feature from the images of the solar observatory. Interestingly, the implementation of the developed approach one to track the sun's activity in the images of the solar observatory revealed that the model accurately captures the areas of the images associated with solar storms where the magnetic field lines are notably obvious. In the areas where is no indication of solar stormy activities, the model did not spot any features in the solar observatory images.

We noticed that the computational time for the entropy measures to obtain information from the solar observatory images is more compared to the computation time spent on statistical tools. Interestingly, both measures of approach one accurately tracks the areas of the solar storms in the solar observatory image. As we know that the imagery system of the solar observatory is continuously rotating with respect to time. As a result, the feature extraction obtained from the 1-DTS of the solar observatory image was subjected to rotational transformation test. The result of the stability checking of the feature extraction through statistical and entropy measure to rotational transformation revealed that the model (Approach 1) is effective to rotational effect of the images with evidence of high value of classification accuracy. In the direct classification method (Approach 2) similar evidence of high value of classification accuracy in tracking the sun's activity in the solar observatory image is observed. Notably, the Approach 2 model achieve a better accuracy in the training comparing to Approach 1. We noticed that the direct classification

method has less resistance to rotational transformation when subjected to stability checking. However, introducing an extended database after training enhances the stability checking of the direct classification method. As a result of the study, we found that both approach model is robust to rotational transformation.

The trend of the 1-DTS obtained from the solar observatory image corresponding to the areas of solar storm is noticed to depicts an enhancement in amplitude changes. This observation may be due to the periodicity of magnetic field pattern and their twisting. While the 1-DTS obtained from the solar observatory image corresponding to no solar storm (i.e., quiet sun activity) depicts a reduction in amplitude with an irregular trend of wave pattern. Furthermore, the entropy obtained from the 1-DTS corresponding to the solar storm areas depicts low values of SVDEn. This actually signifies that during solar storms, a low value of entropy is experienced while at no solar storm areas, the SVDEn depict high entropy values. This features of entropy is in agreement to the entropy observation during geomagnetic storms [30–32].

5 Conclusion

This study had developed two approaches of tracking the sun's activity from the solar observatory images. The images obtained from the solar observatory are transform to one-Dimensional Time Series using 2D circular kernel time series transformation. The first approach applied the statistical and entropy measures while the second approach applied Direct time series method for ML classification to capture the solar storms and no solar storm area in the images of the solar observatory. Interestingly, both approaches give acceptable results which consistently classifies areas of the solar observatory images with swirling magnetic field lines associated with solar storm. They are resistant to image rotation, glare, and optical artifacts. When processing large volumes of solar observatory images, the second approach has the advantage of classifying pixels in a single image 16 times faster. The first approach is generally more robust to rotational transformation and requires less training set to achieve $T_{90^\circ}=0.99$ compared to the second approach. When using an extended database, the second approach gives the highest possible value of $T_{90^\circ}=1$. The SVDEn captures the best accurate features extraction from the images of solar observatory and revealed low values of entropy in the areas with solar storm. While the 5th percentile (X_{SP}) depicts the strongest feature extraction obtained from the solar observatory images. Finally, both approaches perform excellently in tracking the sun activity from the solar observatory images.

Supplementary Materials: Images.zip – 10 files with different solar activity

Author Contributions: Conceptualization, I.A.O and A.V.; methodology, I.A.O, A.V., and M.B.; software, A.V. and M.B.; validation, I.A.O., A.V., M. B., and O.I.O; formal analysis, I.A.O., A.V., and M.B; investigation, I.A.O and A.V; resources, A.V. and I.A.O; data curation, I.A.O., and A.V; writing—original draft preparation, I.A.O., A.V., M.B., and I.O.O; writing—review and editing, I.A.O., A.V., M.B., and O.I.O; visualization, I.A.O., and A.V.; supervision, I.A.O, and A.V.; project administration, I.A.O and A.V.; funding acquisition, A.V. All authors have read and agreed to the published version of the manuscript.

Funding: This research was supported by the Russian Science Foundation (grant no. 22-11-00055, <https://rscf.ru/en/project/22-11-00055/>, accessed on 30 March 2023)

Data Availability Statement: The solar observatory images used in this study can be access through the archive of NASA, Solar Dynamic Observatory (SDO), <https://sdo.gsfc.nasa.gov/data/ai-ahmi/browse/queued.php>.

Acknowledgments: The authors would like to acknowledge the National Aeronautics and Space Administration, Space Physics Facility (NASA), Solar Dynamics Observatory for making the solar observatory images available for research purpose.

Conflicts of Interest: The authors declare no conflict of interest

References

1. To, W.; Space, I.; Forecasting, W.; Sun, T.; Carrington, T.; Weather, S. Understanding the Sun's (Magnetic) Weather To Improve Space Weather Forecasting. **1859**.
2. Kucuk, A.; Banda, J.M.; Angryk, R.A. A Large-Scale Solar Dynamics Observatory Image Dataset for Computer Vision Applications. *Sci. Data* **2017**, *4*, 1–9, doi:10.1038/sdata.2017.96.
3. Zharkov, S.; Zharkova, V.; Ipson, S.; Benkhalil, A. Technique for Automated Recognition of Sunspots on Full-Disk Solar Images. *EURASIP J. Appl. Signal Processing* **2005**, *2005*, 2573–2584, doi:10.1155/ASP.2005.2573.
4. Lee, C.D.; Huang, H.C.; Yeh, H.Y. The Development of Sun-Tracking System Using Image Processing. *Sensors (Switzerland)* **2013**, *13*, 5448–5459, doi:10.3390/s130505448.
5. Yu, L.; Deng, L.; Feng, S. Automated Sunspot Detection Using Morphological Reconstruction and Adaptive Region Growing Techniques. *Proc. 33rd Chinese Control Conf. CCC 2014* **2014**, 7168–7172, doi:10.1109/ChiCC.2014.6896184.
6. Zhao, C.; Lin, G.; Deng, Y.; Yang, X. Automatic Recognition of Sunspots in HSOS Full-Disk Solar Images. *Publ. Astron. Soc. Aust.* **2016**, *33*, doi:10.1017/pasa.2016.17.
7. Baso, C.J.D.; Ramos, A.A. Enhancing SDO/HMI Images Using Deep Learning. *Astron. Astrophys.* **2018**, *614*, 1–13, doi:10.1051/0004-6361/201731344.
8. Ishikawa, S. nosuke; Matsumura, H.; Uchiyama, Y.; Glesener, L. Automatic Detection of Occulted Hard X-Ray Flares Using Deep-Learning Methods. *Sol. Phys.* **2021**, *296*, doi:10.1007/s11207-021-01780-x.
9. Quan, L.; Xu, L.; Li, L.; Wang, H.; Huang, X. Solar Active Region Detection Using Deep Learning. *Electron.* **2021**, *10*, 1–10, doi:10.3390/electronics10182284.
10. Yang, Y.; Yang, H.; Bai, X.; Zhou, H.; Feng, S.; Liang, B. Automatic Detection of Sunspots on Full-Disk Solar Images Using the Simulated Annealing Genetic Method. *Publ. Astron. Soc. Pacific* **2018**, *130*, 104503, doi:10.1088/1538-3873/aadbfa.
11. Armstrong, J.A.; Fletcher, L. Fast Solar Image Classification Using Deep Learning and Its Importance for Automation in Solar Physics. *Sol. Phys.* **2019**, *294*, doi:10.1007/s11207-019-1473-z.
12. Zhu, G.; Lin, G.; Wang, D.; Liu, S.; Yang, X. Solar Filament Recognition Based on Deep Learning. *Sol. Phys.* **2019**, *294*, 1–13, doi:10.1007/s11207-019-1517-4.
13. Love, T.; Neukirch, T.; Parnell, C.E. Analyzing AIA Flare Observations Using Convolutional Neural Networks. *Front. Astron. Sp. Sci.* **2020**, *7*, 1–8, doi:10.3389/fspas.2020.00034.
14. Sarsembayeva, A.; Odsuren, M.; Belisarova, F.; Sarsembay, A.; Maftunzada, S.A.L. Detecting the Sun's Active Region Using Image Processing Techniques. *Phys. Sci. Technol.* **2021**, *8*, 48–53, doi:10.26577/phst.2021.v8.i2.07.
15. Abed, A.K.; Qahwaji, R.; Abed, A. The Automated Prediction of Solar Flares from SDO Images Using Deep Learning. *Adv. Sp. Res.* **2021**, *67*, 2544–2557, doi:10.1016/j.asr.2021.01.042.
16. Velichko, A.; Belyaev, M.; Wagner, M.P.; Taravat, A. Entropy Approximation by Machine Learning Regression: Application for Irregularity Evaluation of Images in Remote Sensing. *Remote Sens.* **2022**, *14*, doi:10.3390/rs14235983.
17. Velichko, A.; Wagner, M.P.; Taravat, A.; Hobbs, B.; Ord, A. NNetEn2D: Two-Dimensional Neural Network Entropy in Remote Sensing Imagery and Geophysical Mapping. *Remote Sens.* **2022**, *14*, doi:10.3390/rs14092166.
18. Ali, Z.; Bhaskar, S.B. Basic Statistical Tools in Research and Data Analysis. *Indian J. Anaesth.* **2016**, *60*, 662–669, doi:10.4103/0019-5049.190623.
19. Velichko, A.; Heidari, H. A Method for Estimating the Entropy of Time Series Using Artificial Neural Networks. *Entropy* **2021**, *23*.
20. Ponce-Flores, M.; Frausto-Solís, J.; Santamaría-Bonfil, G.; Pérez-Ortega, J.; González-Barbosa, J.J. Time Series Complexities and Their Relationship to Forecasting Performance. *Entropy* **2020**, *22*.
21. Sabatini, A.M. Analysis of Postural Sway Using Entropy Measures of Signal Complexity. *Med. Biol. Eng. Comput.* **2000**, *38*,

- 617–624, doi:10.1007/BF02344866.
22. Jelinek, H.F.; Donnan, L.; Khandoker, A.H. Singular Value Decomposition Entropy as a Measure of Ankle Dynamics Efficacy in a Y-Balance Test Following Supportive Lower Limb Taping. *Proc. Annu. Int. Conf. IEEE Eng. Med. Biol. Soc. EMBS* **2019**, 2439–2442, doi:10.1109/EMBC.2019.8856655.
 23. Espinosa-Paredes, G.; Rodriguez, E.; Alvarez-Ramirez, J. A Singular Value Decomposition Entropy Approach to Assess the Impact of Covid-19 on the Informational Efficiency of the WTI Crude Oil Market. *Chaos, Solitons and Fractals* **2022**, *160*, 112238, doi:10.1016/j.chaos.2022.112238.
 24. Bandt, C.; Pompe, B. Permutation Entropy: A Natural Complexity Measure for Time Series. *Phys. Rev. Lett.* **2002**, *88*, 174102, doi:10.1103/PhysRevLett.88.174102.
 25. Chanwimalueang, T.; Mandic, D.P. Cosine Similarity Entropy: Self-Correlation-Based Complexity Analysis of Dynamical Systems. *Entropy* **2017**, *19*, doi:10.3390/e19120652.
 26. Chen, Z.; Li, Y.; Liang, H.; Yu, J. Hierarchical Cosine Similarity Entropy for Feature Extraction of Ship-Radiated Noise. *Entropy* **2018**, *20*, doi:10.3390/e20060425.
 27. Buisine, J.; Bigand, A.; Synave, R.; Delepouille, S.; Renaud, C. Stopping Criterion during Rendering of Computer-Generated Images Based on Svd-Entropy. *Entropy* **2021**, *23*, 1–30, doi:10.3390/e23010075.
 28. Reyes-Lagos, J.J.; Pliego-Carrillo, A.C.; Ledesma-Ramírez, C.I.; Peña-Castillo, M.Á.; García-González, M.T.; Pacheco-López, G.; Echeverría, J.C. Phase Entropy Analysis of Electrohysterographic Data at the Third Trimester of Human Pregnancy and Active Parturition. *Entropy* **2020**, *22*, doi:10.14202/IJOH.2020.76-82.
 29. Simons, S.; Espino, P.; Abásolo, D. Fuzzy Entropy Analysis of the Electroencephalogram in Patients with Alzheimer’s Disease: Is the Method Superior to Sample Entropy? *Entropy* **2018**, *20*, 1–13, doi:10.3390/e20010021.
 30. Oludehinwa, I.A.; Olusola, O.I.; Bolaji, O.S.; Odeyemi, O.O.; Njah, A.N. Magnetospheric Chaos and Dynamical Complexity Response during Storm Time Disturbance. *Nonlinear Process. Geophys.* **2021**, *28*, 257–270, doi:10.5194/npg-28-257-2021.
 31. Balasis, G.; Daglis, I.A.; Papadimitriou, C.; Kalimeri, M.; Anastasiadis, A.; Eftaxias, K. Investigating Dynamical Complexity in the Magnetosphere Using Various Entropy Measures. *J. Geophys. Res. Sp. Phys.* **2009**, *114*, doi:https://doi.org/10.1029/2008JA014035.
 32. Papadimitriou, C.; Balasis, G.; Boutsis, A.Z.; Daglis, I.A.; Giannakis, O.; Anastasiadis, A.; Michelis, P.D.; Consolini, G. Dynamical Complexity of the 2015 St. Patrick’s Day Magnetic Storm at Swarm Altitudes Using Entropy Measures. *Entropy* **2020**, *22*.

Disclaimer/Publisher’s Note: The statements, opinions and data contained in all publications are solely those of the individual author(s) and contributor(s) and not of MDPI and/or the editor(s). MDPI and/or the editor(s) disclaim responsibility for any injury to people or property resulting from any ideas, methods, instructions or products referred to in the content.